



1 **Daytime aerosol optical depth above low-level**
2 **clouds is similar to that in adjacent clear skies**
3 **at the same heights: airborne observation**
4 **above the southeast Atlantic**

5 Yohei Shinozuka^{1,2}, Meloë S. Kacenelenbogen², Sharon P. Burton³, Steven G. Howell⁴, Paquita
6 Zuidema⁵, Richard A. Ferrare³, Samuel E. LeBlanc^{2,6}, Kristina Pistone^{2,6}, Stephen Broccardo^{1,2},
7 Jens Redemann⁷, K. Sebastian Schmidt⁸, Sabrina P. Cochrane^{8,9}, Marta Fenn^{3,10}, Steffen Freitag⁴,
8 Amie Dobracki^{4,5}, Michal Segal-Rosenheimer^{2,6,11}, Connor J. Flynn⁷

9

10 ¹ Universities Space Research Association, Columbia, Maryland, USA

11 ² NASA Ames Research Center, Moffett Field, California, USA

12 ³ NASA Langley Research Center, Hampton, Virginia, USA

13 ⁴ University of Hawaii at Manoa, Honolulu, Hawaii, USA

14 ⁵ University of Miami, Miami, Florida, USA

15 ⁶ Bay Area Environmental Research Institute, Moffett Field, California, USA

16 ⁷ University of Oklahoma, Norman, Oklahoma, USA

17 ⁸ University of Colorado, Boulder, Colorado, USA

18 ⁹ Laboratory for Atmospheric and Space Physics, Boulder, Colorado, USA

19 ¹⁰ Science Systems and Applications, Inc, Hampton, VA, USA

20 ¹¹ Department of Geophysics, Porter School of the Environment and Earth Sciences, Tel-Aviv
21 University, Tel-Aviv, Israel

22 *Correspondence to:* Y. Shinozuka (Yohei.Shinozuka@nasa.gov)



23 **Abstract**

24 To help satellite retrieval of aerosols and studies of their radiative effects, we demonstrate
25 that daytime 532 nm aerosol optical depth over low-level clouds is similar to that in neighboring
26 clear skies at the same heights in recent airborne lidar and sunphotometer observations above the
27 southeast Atlantic. The mean AOD difference is between 0 and -0.01, when comparing the cloudy
28 and clear sides, each up to 20 km wide, of cloud edges. The difference is not statistically significant
29 according to a paired t-test. Systematic differences in the wavelength dependence of AOD and in
30 situ single scattering albedo are also minute. These results hold regardless of the vertical distance
31 between cloud top and aerosol layer bottom. AOD aggregated over $\sim 2^\circ$ grid boxes for each of
32 September 2016, August 2017 and October 2018 also shows little correlation with the presence of
33 low-level clouds. We posit that a satellite retrieval artifact is entirely responsible for a previous
34 finding of generally smaller AOD over clouds (Chung et al., 2016), at least for the region and time
35 of our study. Our results also suggest that the same values can be assumed for the intensive
36 properties of free-tropospheric biomass-burning aerosol regardless of whether clouds exist below.

37 **1. Introduction**

38 A significant amount of atmospheric particles are transported above liquid water clouds on
39 the global scale (Waquet et al., 2013). Aerosols above clouds (AAC) may influence the climate in
40 three ways. Their light absorption is amplified by cloud reflection. The heating of the atmosphere
41 due to the absorption may stabilize the atmosphere. The particles may eventually subside, enter
42 clouds and alter their properties. Estimates of the direct aerosol radiative effect alone see large
43 inter-model spread for areas with large aerosol optical depth (AOD) over widespread clouds (Stier
44 et al., 2013; Zuidema et al., 2016).

45 Since AAC are difficult to see from the ground or a ship, previous studies have relied on
46 satellite observations (see Table 2 of Kacenelenbogen et al., 2019). Among them is Chung et al.
47 (2016), which used the level 2 products of the Cloud-Aerosol Lidar with Orthogonal Polarization
48 (CALIOP) (Winker et al., 2009) to calculate the AOD above the maximum low-cloud-top-height
49 in each grid cell in clear sky as well as the AOD above low clouds on a global $2^\circ \times 5^\circ$ latitude–
50 longitude grid. Their results indicate that daytime 532 nm AOD above low clouds is generally



51 lower than that in clear sky at the same heights. The difference is up to 0.04 over the southeastern
52 Atlantic Ocean (see their Fig. 2)

53 As Chung et al. (2016) point out, it is conceivable that aerosol amounts over cloud can be
54 different from those in nearby clear sky. There are two sets of potential reasons. The first concerns
55 the effects of meteorology. Large-scale circulation patterns paired with solar reflection from clouds
56 on aerosols could modify the horizontal and vertical extent of aerosols, aerosol concentration and
57 chemical composition. For example, the properties of hygroscopic aerosols might vary if the
58 relative humidity in clear skies is somehow higher than above clouds. The second set of reasons
59 pertain to the case of aerosols in close proximity to clouds. The proximity has been variously
60 defined, for example less than 100 m in the vertical direction (Costantino and Bréon, 2013) and
61 less than 20 km in the horizontal direction (Várnai and Marshak, 2018). Chung et al. (2016) note
62 that aerosols were shown to influence underlying cloud by indirect effects and semidirect effects
63 (Costantino and Bréon, 2010, 2013; Johnson et al., 2004; Wilcox, 2010) and that these aerosol–
64 cloud interactions and possibly more (e.g., a pronounced if unlikely aerosol entrainment (Diamond
65 et al., 2018)) might somehow affect the aerosol amount over cloud. A bias in the CALIOP standard
66 retrieval was also raised as a possible explanation for the Chung et al. (2016) results. The detection
67 threshold in the feature detection algorithm varies depending on the background lighting
68 conditions, the atmospheric features (e.g., aerosols, high altitude cirrus or boundary layer clouds)
69 and the horizontal averaging required by CALIOP for detection (see Fig. 4 of Winker et al. (2009)).
70 In the particular case of aerosols above clouds, Kacenelenbogen et al. (2014) show that the
71 CALIOP standard algorithm substantially underestimates the frequency of AAC when the AOD
72 is less than ~ 0.02 . This is due mostly to tenuous aerosols with a backscatter under the detection
73 threshold; however, Kacenelenbogen et al. (2014) saw no clear bias in AOD above clouds between
74 CALIOP and the NASA Langley airborne High Spectral Resolution Lidar (HSRL-1). Liu et al.
75 (2015) show a clear AOD underestimate of the CALIOP level 2 retrieval in comparison to a
76 separate retrieval after Hu et al. (2007) for smoke above opaque water clouds over the southeast
77 Atlantic, and explain this by the CALIOP layer detection scheme prematurely assigning layer base
78 altitudes and thus underestimating the geometric thickness of smoke layers. According to Chung
79 et al. (2016), the negative daytime AOD differences between cloudy and cloud-free conditions
80 “might simply be a result of systematic differences between the detection thresholds in clear sky



81 and above low bright clouds”. The authors add that the bias may be enhanced over the ocean due
82 to the lower albedo compared to that of land.

83 The subject warrants further investigation, given the importance of AAC on climate. An
84 airborne experiment can help by providing direct measurements that are subject to smaller
85 uncertainty, in finer spatial and temporal resolution albeit over limited ranges. The NASA
86 Observations of Aerosols above CLouds and their intEractionS (ORACLES) mission was carried
87 out to study key processes that determine the climate impacts of African biomass-burning aerosols
88 above the southeast Atlantic. Of the two deployed aircraft, the NASA P3, equipped with in situ
89 and remote sensing instruments, flew in the lower- to mid-troposphere, mostly in September 2016,
90 August 2017 and October 2018. In September 2016 the NASA ER2 also flew, at about 20 km
91 altitude with downward-viewing sensors. Extensive stratocumulus clouds were observed
92 repeatedly throughout the mission; see a sample satellite image in Redemann et al. (in preparation).
93 Details of the ORACLES mission can be found in Redemann et al. (in preparation), Zuidema et
94 al. (2016) and Shinozuka et al. (2019).

95 The instrumentation relevant to the present paper is described in Sect. 2 along with
96 sampling and statistical hypothesis testing methods. This is followed by comparisons of AOD and
97 other aerosols properties above the height of cloud top between cloudy and clear skies (Sect. 3).
98 Sect. 4 offers discussion.

99 2. Methods

100 2.1. Instrumentation

101 The remote sensing and in situ instruments used in this study are briefly described below
102 with references to full descriptions. Note that the measurements each refer to a unique vertical
103 range, as summarized in Table 1.

104 The NASA Langley Research Center High Spectral Resolution Lidar (HSRL-2), deployed
105 from the ER2 in 2016 and from the P3 in 2017 and 2018, measures calibrated, unattenuated
106 backscatter and aerosol extinction profiles below the instrument. The data are reported with 10 s
107 intervals. The HSRL-2 signal-to-noise ratio is higher than that of CALIOP, due to the much lower
108 altitude and the inverse square dependence of light intensity. In addition, by the use of a second
109 channel to assess aerosol attenuation, the HSRL technique (Shipley et al., 1983) results in an
110 accurate aerosol extinction product with no assumptions about lidar ratio, and also a more accurate



111 backscatter product, particularly in the lower atmosphere where attenuation by upper layers can
112 present difficulties for the spaceborne backscatter lidar. Differences in algorithm are discussed in
113 Sect. 4. Further details about the instrument, calibration and uncertainty can be found in Hair et al.
114 (2008), Rogers et al. (2009) and Burton et al. (2018).

115 Our analysis utilizes the HSRL-2 standard products of cloud top height (CTH), 532 nm
116 particulate backscattering and 532 nm aerosol optical thickness (Burton et al., 2012) in three ways.
117 First, flight segments are isolated using the CTH product (detailed in Sect. 2.2). Second, the bottom
118 and top heights of the smoke plumes are defined with a (somewhat arbitrarily chosen) threshold
119 backscattering coefficient at $0.25 \text{ Mm}^{-1}\text{sr}^{-1}$ after Shinozuka et al. (2019).

120 Third, we evaluate the 532 nm partial-column aerosol optical thickness from below the
121 aircraft down to ~ 50 m above the CTH, (even for columns without clouds; see Sect. 2.2). The ~ 50 -
122 m buffer is designed to reduce the ambiguity associated with the transition at the cloud top. The
123 upper limit of the integral of extinction is 14 km altitude for the 2016 ER2 flights and 1500 m
124 below the P3 altitude for 2017 and 2018. Profiles with possible influences of mid- and high-level
125 clouds are largely excluded from the product, though isolated cases of thin clouds may remain.

126 We also use partial-column AOD observed upward from the P3 with a sunphotometer. The
127 Spectrometer for Sky-Scanning, Sun-Tracking Atmospheric Research (4STAR) measures hyper-
128 spectral direct solar beam. Calculated AOD is reported at 1 Hz. Our analysis excludes data with
129 possible influences of clouds above the instrument. Further details on the instrument as well as
130 data acquisition, screening, calibration and reduction can be found in Dunagan et al. (2013),
131 Shinozuka et al. (2013) and LeBlanc et al. (2019).

132 For 2017 and 2018, we examine a combination of the 4STAR and HSRL-2 AODs, in order
133 to cover the free troposphere both upward and downward from the aircraft that flew in it (Fig. 1).
134 The vertical coverage is compromised by two limitations intrinsic to the lidar measurements. First,
135 the CTH is not sought within 500 m of the instrument (not to be confused with the ~ 50 -m lower
136 buffer for the extinction integral). This means that the flight segments with clouds so close to the
137 aircraft enter our analysis only if the clouds extended as deep as to reach 500 m away from it. This
138 is at most a minor fraction of the data, as the fraction with the CTH within 550 m of the P3 altitude
139 is a mere 3%. Second, because of the 1500 m upper buffer for the extinction integral, we only have
140 4STAR above-P3 AOD for the flight segments when the plane was 500-1500 m above the CTH



141 (Fig. 1b). We add the HSRL-2 AOD to the 4STAR AOD only for the flight segments when the P3
142 was >1500 m above the CTH (Fig. 1c).

143 For 2016, we examine the HSRL-2 AOD only, because, with the lidar above the
144 troposphere, two of the missing layers can safely be ignored, leaving the ~50 m lower buffer as
145 the only missing layer (Fig. 1a). We refer to all these AODs from the three campaigns collectively
146 as AOD_{ct} (see Table 1). The wavelength dependence expressed as Angstrom exponent is calculated
147 for 10-s periods with AOD_{ct} at 355 and 532 nm both exceeding 0.1.

148 In situ aerosol instruments operated from the P3 include a nephelometer (TSI model 3563)
149 and a particle soot absorption photometer (PSAP, Radiance Research 3-wavelength version),
150 which measure particulate light scattering and absorption, respectively. After adjustments are
151 made for factors such as angular truncations (Anderson and Ogren, 1998) and filter interference
152 (Virkkula, 2010) for each wavelength, extinction coefficient and single scattering albedo at 550
153 nm are derived for an instrument relative humidity (RH) that is typically below 40%. Pistone et al.
154 (2019) and Shinozuka et al. (2019) have more details. The non-refractory masses of submicron
155 particles were measured by a time-of-flight aerosol mass spectrometer (Aerodyne, Inc HR-ToF
156 AMS, DeCarlo et al. (2006)). A condensation particle counter (TSI model 3010, with ΔT set to
157 22°C) measured the number concentration of particles larger than about 10 nm. These in situ
158 properties refer to the air immediately outside the P3 aircraft, not a vertical column. Only the in
159 situ measurements in 2017 and 2018 at 500-1500 m above the CTH are used in this study.

160 **2.2. Sampling**

161 Two methods are employed for selecting subsets of the observations for analysis. In the
162 first (Sect. 2.2.1), we bundle data from areas hundreds of kilometers wide for each of the three
163 campaigns, in a manner as similar to the CALIOP-based study (Chung et al., 2016) as the airborne
164 measurements allow. In the second method (Sect. 2.2.2), we pair cloudy and clear skies with more
165 stringent spatiotemporal criteria to isolate the impact of finer-scale phenomena. Note that both
166 methods ignore time periods for which the 532 nm backscattering product (from which the CTH
167 product is derived) is masked at all altitudes, as well as transit flights into and out of the study area.
168 Cases are also excluded where the CTH exceeds 3241 m. This is to be consistent with the study
169 by Chung et al. (2016), which refers to clouds at 680 hPa or higher pressure, although we find
170 similar results with or without this restriction.



171 **2.2.1. Meso-scale monthly-mean sampling**

172 This method separates profiles measured in the three campaigns into two groups: those
173 concurrent with a presence of low-level clouds as reported by the HSRL-2 and those concurrent
174 with an absence of any cloud detected by HSRL-2 in the column. The groups are each aggregated
175 into grid boxes approximately 2° by 2°, as shown in Fig. 2. This grid is adapted from Shinozuka et
176 al. (2019) but with additional boxes for the São Tomé-based 2017 and 2018 campaigns. In total,
177 109 hours and 39 hours of flight segments are selected for the cloudy and clear groups,
178 respectively, including minor double-counting where boxes overlap.

179 The arithmetic mean of the CTH of the cloudy group is calculated for each day for each
180 box and 50 m above it is set as the lowest altitude for computing AOD_{ct} for each 10 s period (Sect.
181 2.1). Then the arithmetic mean and standard deviation are calculated for the AOD_{ct}, as well as
182 other measurements (Sect. 2.1, Table 1), for each group and each box. After excluding the time
183 periods with mid- and high-level clouds and instrument/aircraft issues, 49 hours and 26 hours of
184 the AOD_{ct} measurements enter the analysis for cloudy and clear-sky groups, respectively.

185 **2.2.2. Local-scale near-synchronous sampling**

186 This method identifies cloud edges and demarcates the cloudy side and clear side of each
187 edge based on the time series of the CTH detected by HSRL-2, for level flight legs only. Cloud
188 edges are defined by the points in time when a cloud is detected in a profile adjacent to a profile
189 with no cloud detection.

190 A clear sky and a cloud are represented by the time period of a certain length, say 60 s,
191 preceding each edge and the same length following it. To ensure that clear skies and clouds are
192 not interrupted for the length, we exclude edges for which another one is found within the length.
193 The longer the length, the smaller the number of cloudy-clear pairs, because longer continuous
194 clouds and clear skies are rarer. Furthermore, we set another length, 20 s in the example illustrated
195 in Fig. 3a, to exclude immediately before and after the edge, in order to reduce ambiguity
196 associated with a gradual transition from cloud droplets to unactivated particles, the so-called
197 twilight zone (Koren et al., 2007; Schwarz et al., 2017; Várnai and Marshak, 2018). We convert
198 the temporal dimensions into horizontal ones using the mean true horizontal aircraft speed, 200
199 ms⁻¹ for the ER2 (Fig. 3a) and 140 ms⁻¹ for the P3 (Fig. 3b and Fig. 3c).



200 We change both the maximum and minimum limits of separation, in order to assess scale
201 dependence and sampling error as much as our airborne data permit. The way the edges are
202 identified ensures that a measurement cannot be counted more than twice for a given range of
203 separation. A measurement can, however, enter multiple ranges of separation. For example, a
204 measurement 4-6 km away from a cloud edge enters the ranges of 0-6 km, 2-6 km, 2-12 km, 4-12
205 km, 4-24 km, etc. In total, 5.0 hours of horizontal flight are selected, including the double-counting
206 for a given range but excluding the multiple-counting over multiple ranges. Exactly half of them
207 are over clouds. Note that these expressions of separation are only notional; we discuss this in Sect.
208 4.

209 As with the meso-scale monthly-mean sampling, we take the arithmetic mean of the CTH
210 of the cloudy side and add 50 m (red lines in Fig. 3). The height is extended to the adjacent clear
211 sky (orange lines) for the calculation of AOD_{ct} (Sect. 2.1). The in situ measurements (Sect. 2.1,
212 Table 1) are each averaged over the cloudy sides and over the clear sides. Cases where aerosol
213 measurements are unavailable for 33% or more of the time period, for example due to calibration
214 or operation problems, are excluded. This makes the number of cloudy-clear pairs vary from
215 property to property for a given range of separation. In total, 3.8 hours of AOD_{ct} measurements
216 enter the analysis.

217 **2.3. Statistical hypothesis testing**

218 We employ the paired t-test, also called paired-samples t-test or dependent t-test, to
219 determine whether the mean difference in each property (e.g., AOD_{ct}) between the presence and
220 absence of low-level clouds is statistically consistent with the null hypothesis of zero difference.
221 The procedure entails calculating the t statistic, the ratio of the mean cloudy-clear differences to
222 their standard error. Here the standard error is the standard deviation computed for $N-1$ degrees of
223 freedom divided by the square root of N , where N is the number of sample pairs. Note that the
224 standard deviation is close to the root-mean-square deviation (RMSD) for small absolute mean
225 difference, unless N is smaller than five.

226 For the calculated t statistic, the two-tailed p value is looked up. Small p values are
227 associated with large t statistics and hence generally large mean differences relative to RMSD. If
228 the p value is smaller than 0.05, we reject the null hypothesis. If it is greater, we do not.



229 The procedure makes several assumptions. One is independence of the differences.
230 Synoptic- and meso-scale phenomena prevalent throughout ORACLES (e.g., subsidence and
231 anticyclones) reduce the independence of the samples. The low day-to-day meteorological
232 variability and repeated flight paths might mean that the same aerosol-cloud conditions were
233 sampled day after day. It is unclear whether this would reduce the independence of the cloudy-
234 clear differences - a potential, seemingly untestable caveat for the meso-scale monthly-mean
235 sampling (Sect. 2.2.1). In the local scale the exclusion of contiguous cloud edges (Sect. 2.2.2)
236 should attain a high level of independence from one another. The procedure also assumes
237 continuous (not discrete), approximately normally distributed data free of outliers.

238 **3. Results**

239 The meso-scale monthly-mean method finds little systematic difference in 532 nm AOD_{ct}
240 (Fig. 4). Most markers lie near the 1:1 line. The mean difference, an indicator of systematic
241 differences, is +0.02. This is only +16% of the RMSD, an indicator of the total (random and
242 systematic) variability. The p value from the paired t-test is 0.23. Thus, the AOD above low-level
243 clouds is not significantly different from that at the same heights above nearby clear skies in this
244 scale. The p value is also greater than 0.05 for \log_{10} of AOD_{ct} , the Angstrom exponent and in situ
245 aerosol properties (Table 2, see the rows labeled “box means”).

246 The only exception is the particle number concentration. Four of the 32 horizontal boxes
247 see 3-7 times as large concentration over clouds as that over neighboring clear skies (4600-5700
248 cm^{-3} vs. 700-2100 cm^{-3}). The mean cloudy-clear difference among all box means is about +40%
249 of the RMSD. The t-test yields a p value of 0.01. One of the assumptions underlying the test, the
250 absence of outliers, may be broken in this case.

251 The local-scale near-synchronous method finds virtually the same results. The AOD_{ct} is
252 compared in Fig. 5a for 2-6 km separation. The time period corresponds to approximately 10-30 s
253 temporal range on the ER2 (13 data points from the 2016 campaign) and 14-43 s at the average P3
254 speed (53 from 2017 and 2018). All data points lie near the 1:1 line. The mean difference, -0.002,
255 is only -21% of the RMSD for 2-6 km separation. The p value is 0.08.

256 We run the same calculation for other combinations of minimum and maximum separation.
257 Fig. 6 shows the resulting statistics. The mean difference for 2-6 km separation, for example, is
258 represented in Fig. 6a at maximum separation (x axis) of 6 km by the solid orange line that starts



259 after the minimum separation of 2 km. This line also shows that the mean difference is -0.01 if the
260 maximum separation is set to 20 km while keeping the minimum at 2 km. The longest blue line
261 represents the calculations for zero minimum separation (i.e., with the twilight zone included). All
262 other solid lines represent the results with greater minimum separation. For example, the green
263 line that is missing data up to 4 km indicates that the mean difference is closer to -0.01 at 12 km,
264 as shown in Fig. 5b.

265 For the separation up to 20 km, the mean difference is mostly between 0 and -0.01. The p
266 value, shown in Fig. 6b, is below 0.05 for only a handful of the ranges of separation, many with
267 minimum separation of 0-2 km. This is also true for \log_{10} of AOD_{ct} , the Angstrom exponent and
268 in situ aerosol properties including the number concentration (Table 2). Large p values are also
269 found for the ER2- and P3-borne measurements separately and for the 4STAR and the HSRL-2
270 AOD separately for 2017 and 2018.

271 4. Discussion and Conclusions

272 Virtually no systematic differences in aerosol properties are found between the air above
273 low-level clouds and that above clear areas nearby in ORACLES daytime airborne measurements.
274 The finding holds for a range (0-20 km) of distances between, and expanses of, the two air masses.
275 Note that the temporal and horizontal dimensions associated with the local-scale near-synchronous
276 sampling must be collectively overestimated, because the aircraft may have been running parallel
277 to cloud edge. There is no easy way to know how far from the nearest cloud edge the airplane was
278 in reality. Images from cameras on the plane and satellites may give some context. But we stop
279 short of examining them, discouraged by the perceived difficulty in unifying definition of cloud
280 edges between the cameras and the lidar, among other image processing issues. Although we do
281 not know what the real distances and expanses are, that probably does not matter for the region
282 and season of our study, judging by the consistently large p values across the notional distances
283 and expanses. The meso-scale monthly-average sampling, resting on larger data, provides
284 consistent results. Note that this conclusion may or may not apply to environment elsewhere with
285 less uniform clouds.

286 Our analysis does not support aerosol-cloud interactions, circulation patterns or anything
287 else as a cause for a significant systematic difference, simply because such a difference is not
288 evident. The lack of obvious sensitivity to the smoke-cloud gap height, indicated by marker color



289 in Fig. 5, is consistent with this conclusion. The smoke bottom height minus the mean CTH gives
290 an estimate of whether aerosols may be physically in contact with clouds and therefore there is a
291 chance of wet removal. Our analysis does not detect any sign of local aerosol removal by the
292 underlying clouds.

293 An important difference between the present analysis and the CALIOP-based one (Chung
294 et al., 2016), apart from the spatiotemporal range and resolution, is that the HSRL algorithm (Hair
295 et al., 2008) does not use any explicit layer detection. The return signal in the molecular signal
296 provides a measure of the aerosol attenuation and extinction. A very tenuous aerosol layer still
297 produces a reported extinction with a reported error bar. If the aerosol extinction is very small, the
298 error bar may exceed the retrieved value, but there is no cutoff at small values that produces the
299 kind of bias one gets from a detection threshold. Furthermore, the signal-to-noise is higher than
300 that of CALIOP, as explained in Sect. 2.1.

301 We posit that the systematic differences shown in Chung et al. (2016) are solely a CALIOP
302 retrieval artifact, at least for the ORACLES region and season. As the authors discuss, the CALIOP
303 standard algorithm has a detection bias. The algorithm confines itself to distinct aerosol layers
304 whose signals are high enough compared to detector noise and, during the day, solar background
305 light. If the signal-to-noise ratio of a layer is not high enough, no extinction is reported for the
306 portion of the aerosol profile; summing up the extinction produces a low-biased AOD.

307 The depolarization/multiple scattering method by Hu et al. (2007) retrieves above-cloud
308 AOD from CALIOP without a layer detection algorithm. This method may lead to a different result
309 from Chung et al. (2016). A future study based on the Hu et al. method and extended to the globe
310 as in Kacenelenbogen et al. (2019) will also address environment under a wider variety of synoptic-
311 and meso-scale conditions that produce specific opaque water clouds.

312 The absence of systematic differences is good news, because satellite retrievals and studies
313 of radiative effects do not need to treat these two conditions as different. Our results on AOD_{ct}
314 justify, for example, temporal and horizontal extrapolation of above-cloud AOD to adjacent clear
315 skies and attribution of the difference from full-column AOD to the planetary boundary layer. Our
316 results on the aerosol intensive properties suggest that a single set of aerosol models can be used
317 for the aerosols in the free troposphere regardless of whether clouds exist below, which may allow
318 better characterization of the underlying clouds and the radiative effects (Matus et al., 2015; Meyer
319 et al., 2015). It seems reasonable to use aerosol properties retrieved in clear skies for estimating



320 the direct radiative effects of aerosols above nearby clouds. But challenges remain. Random
321 variability in AOD and other aerosol properties is significant, as indicated by RMSD in the present
322 study and quantified for smoke elsewhere (Shinozuka and Redemann, 2011). It may be
323 problematic to assume the same values for intensive properties for reasons not investigated here,
324 for example: form of combustion, degree of aerosol ageing and influence of the boundary layer.
325 These may be tackled more effectively by combining sensors of various capabilities with improved
326 spatiotemporal resolution and retrieval algorithms (National Academies of Sciences, Engineering,
327 and Medicine et al., 2019). Improved spatiotemporal satellite observations of aerosol properties in
328 clear skies and above clouds are urgently needed to reduce the uncertainty in total aerosol radiative
329 forcing (National Academies of Sciences, Engineering, and Medicine et al., 2019). For this, we
330 are looking forward to the next generation of space-borne lidars, radars, microwave radiometers,
331 polarimeters and spectrometers such as the ones that will address joint Aerosols, Clouds,
332 Convection and Precipitation (ACCP) science goals and objectives ([https://science.nasa.gov/earth-](https://science.nasa.gov/earth-science/decadal-accp)
333 [science/decadal-accp](https://science.nasa.gov/earth-science/decadal-accp))

334 **Data availability**

335 The P3 and ER2 observational data (ORACLES Science Team, 2017, 2019) are available
336 through www.espo.nasa.gov/oracles.

337 **Author contribution**

338 All authors participated in the investigation during the ORACLES intensive observation
339 periods. In addition, MSK led conceptualization, funding acquisition, methodology, project
340 administration and supervision. YS led data curation, formal analysis, software and validation and
341 wrote the original draft. YS and MSK contributed visualization. All but CJF reviewed and edited
342 the manuscript.

343 **Competing interests**

344 The authors declare that they have no conflict of interest.



345 **Acknowledgments**

346 We thank Eric Wilcox, Tamás Várnai and Sasha Marshak for discussion. ORACLES is
347 funded by NASA Earth Venture Suborbital-2 grant NNH13ZDA001N-EVS2.

348 **References**

- 349 Anderson, T. L. and Ogren, J. A.: Determining aerosol radiative properties using the TSI 3563 integrating
350 nephelometer, *Aerosol Sci. Technol.*, 29, 57–69, 1998.
- 351 Burton, S. P., Ferrare, R. A., Hostetler, C. A., Hair, J. W., Rogers, R. R., Obland, M. D., Butler, C. F.,
352 Cook, A. L., Harper, D. B. and Froyd, K. D.: Aerosol classification using airborne High Spectral
353 Resolution Lidar measurements – methodology and examples, *Atmospheric Measurement Techniques*,
354 5(1), 73–98, 2012.
- 355 Burton, S. P., Hostetler, C. A., Cook, A. L., Hair, J. W., Seaman, S. T., Scola, S., Harper, D. B., Smith, J.
356 A., Fenn, M. A., Ferrare, R. A., Saide, P. E., Chemyakin, E. V. and Müller, D.: Calibration of a high
357 spectral resolution lidar using a Michelson interferometer, with data examples from ORACLES, *Appl.*
358 *Opt.*, 57(21), 6061–6075, 2018.
- 359 Chung, C. E., Lewinschal, A. and Wilcox, E.: Relationship between low-cloud presence and the amount
360 of overlying aerosols, *Atmos. Chem. Phys.*, 16(9), 5781–5792, 2016.
- 361 Costantino, L. and Bréon, F.-M.: Analysis of aerosol-cloud interaction from multi-sensor satellite
362 observations, *Geophys. Res. Lett.*, 37(11), doi:10.1029/2009gl041828, 2010.
- 363 Costantino, L. and Bréon, F.-M.: Aerosol indirect effect on warm clouds over South-East Atlantic, from
364 co-located MODIS and CALIPSO observations, *Atmos. Chem. Phys.*, 13(1), 69–88, 2013.
- 365 DeCarlo, P. F., Kimmel, J. R., Trimborn, A., Northway, M. J., Jayne, J. T., Aiken, A. C., Gonin, M.,
366 Fuhrer, K., Horvath, T., Docherty, K. S., Worsnop, D. R. and Jimenez, J. L.: Field-Deployable, High-
367 Resolution, Time-of-Flight Aerosol Mass Spectrometer, *Anal. Chem.*, 78(24), 8281–8289, 2006.
- 368 Diamond, M. S., Dobracki, A., Freitag, S., Small Griswold, J. D., Heikkila, A., Howell, S. G., Kacarab,
369 M. E., Podolske, J. R., Saide, P. E. and Wood, R.: Time-dependent entrainment of smoke presents an
370 observational challenge for assessing aerosol–cloud interactions over the southeast Atlantic Ocean,
371 *Atmos. Chem. Phys.*, 18(19), 14623–14636, 2018.
- 372 Dunagan, S. E., Johnson, R., Zavaleta, J., Russell, P. B., Schmid, B., Flynn, C., Redemann, J., Shinozuka,
373 Y., Livingston, J. and Segal-Rosenhaimer, M.: Spectrometer for Sky-Scanning Sun-Tracking
374 Atmospheric Research (4STAR): Instrument Technology, *Remote Sensing*, 5(8), 3872–3895, 2013.
- 375 Hair, J. W., Hostetler, C. A., Cook, A. L., Harper, D. B., Ferrare, R. A., Mack, T. L., Welch, W.,
376 Izquierdo, L. R. and Hovis, F. E.: Airborne High Spectral Resolution Lidar for profiling aerosol optical
377 properties, *Appl. Opt.*, 47(36), 6734–6752, 2008.
- 378 Hu, Y., Vaughan, M., Liu, Z., Powell, K. and Rodier, S.: Retrieving Optical Depths and Lidar Ratios for
379 Transparent Layers Above Opaque Water Clouds From CALIPSO Lidar Measurements, *IEEE*
380 *Geoscience and Remote Sensing Letters*, 4(4), 523–526, 2007.



- 381 Johnson, B. T., Shine, K. P. and Forster, P. M.: The semi-direct aerosol effect: Impact of absorbing
382 aerosols on marine stratocumulus, *Quarterly Journal of the Royal Meteorological Society*, 130(599),
383 1407–1422, doi:10.1256/qj.03.61, 2004.
- 384 Kacenelenbogen, M., Redemann, J., Vaughan, M. A., Omar, A. H., Russell, P. B., Burton, S., Rogers, R.
385 R., Ferrare, R. A. and Hostetler, C. A.: An evaluation of CALIOP/CALIPSO’s aerosol-above-cloud
386 detection and retrieval capability over North America, *J. Geophys. Res. D: Atmos.*, 119(1), 230–244,
387 2014.
- 388 Kacenelenbogen, M. S., Vaughan, M. A., Redemann, J., Young, S. A., Liu, Z., Hu, Y., Omar, A. H.,
389 LeBlanc, S., Shinozuka, Y., Livingston, J. and Others: Estimations of global shortwave direct aerosol
390 radiative effects above opaque water clouds using a combination of A-Train satellite sensors, *Atmos.*
391 *Chem. Phys.*, 19(7), 4933–4962, 2019.
- 392 Koren, I., Remer, L. A., Kaufman, Y. J., Rudich, Y. and Vanderlei Martins, J.: On the twilight zone
393 between clouds and aerosols, *Geophysical Research Letters*, 34(8), doi:10.1029/2007gl029253, 2007.
- 394 LeBlanc, S. E., Redemann, J., Flynn, C., Pistone, K., Kacenelenbogen, M., Segal-Rosenheimer, M.,
395 Shinozuka, Y., Dunagan, S., Dahlgren, R. P., Meyer, K., Podolske, J., Howell, S. G., Freitag, S., Small-
396 Griswold, J., Holben, B., Diamond, M., Formenti, P., Piketh, S., Maggs-Kölling, G., Gerber, M. and
397 Namwoonde, A.: Above Cloud Aerosol Optical Depth from airborne observations in the South-East
398 Atlantic, , doi:10.5194/acp-2019-43, 2019.
- 399 Liu, Z., Winker, D., Omar, A., Vaughan, M., Kar, J., Trepte, C., Hu, Y. and Schuster, G.: Evaluation of
400 CALIOP 532 nm aerosol optical depth over opaque water clouds, *Atmos. Chem. Phys.*, 15(3), 1265–
401 1288, 2015.
- 402 Matus, A. V., L’Ecuyer, T. S., Kay, J. E., Hannay, C. and Lamarque, J.-F.: The Role of Clouds in
403 Modulating Global Aerosol Direct Radiative Effects in Spaceborne Active Observations and the
404 Community Earth System Model, *J. Clim.*, 28(8), 2986–3003, 2015.
- 405 Meyer, K., Platnick, S. and Zhang, Z.: Simultaneously inferring above-cloud absorbing aerosol optical
406 thickness and underlying liquid phase cloud optical and microphysical properties using MODIS, *J.*
407 *Geophys. Res. D: Atmos.*, 120(11), 5524–5547, 2015.
- 408 National Academies of Sciences, Engineering, and Medicine, Division on Engineering and Physical
409 Sciences, Space Studies Board and Committee on the Decadal Survey for Earth Science and Applications
410 from Space: Thriving on Our Changing Planet: A Decadal Strategy for Earth Observation from Space,
411 National Academies Press., 2019.
- 412 ORACLES Science Team: Suite of Aerosol, Cloud, and Related Data Acquired Aboard ER2 During
413 ORACLES 2016, Version 1, , doi:10.5067/SUBORBITAL/ORACLES/ER2/2016_V1, 2017.
- 414 ORACLES Science Team: Suite of Aerosol, Cloud and Related Data Acquired Aboard P3 During
415 ORACLES 2017, Version 1, , doi:10.5067/SUBORBITAL/ORACLES/P3/2017_V1, 2019.
- 416 Pistone, K., Redemann, J., Doherty, S., Zuidema, P., Burton, S., Cairns, B., Cochrane, S., Ferrare, R.,
417 Flynn, C., Freitag, S., Howell, S. G., Kacenelenbogen, M., LeBlanc, S., Liu, X., Schmidt, K. S., Sedlacek,
418 A. J., III, Segal-Rozenhaimer, M., Shinozuka, Y., Stammes, S., van Diedenhoven, B., Van Harten, G. and
419 Xu, F.: Intercomparison of biomass burning aerosol optical properties from in situ and remote-sensing
420 instruments in ORACLES-2016, *Atmos. Chem. Phys.*, 19(14), 9181–9208, 2019.



- 421 Redemann, Wood, Zuidema, Doherty, Luna, LeBlanc, Diamond, Shinozuka, Ueyama, Pfister, DaSilva,
422 Longo, Kacenelenbogen, Knox, Piketh, Haywood, Formenti, Mallet, Stier, Ackerman, Carmichael, Saide,
423 Howell, Cairns, Knobelspiesse, Tanelli, L'Ecuyer, McFarquhar, Poellot, Nenes, Kacarab, Pui Shan
424 Wong, Small-Griswold, Thornhill, Noone, Podolske, Schmidt, Sedlacek, Lang, Stith, Segal-Rozenhaimer,
425 Hostetler, Ferrare, Burton, Diner, Platnick, Myers, Meyer, Spangenberg, Ian Chang: An overview of the
426 ORACLES (ObseRVations of Aerosols above CLouds and their intEractionS) project: aerosol-cloud-
427 radiation interactions in the Southeast Atlantic basin, in preparation.
- 428 Rogers, R. R., Hair, J. W., Hostetler, C. A., Ferrare, R. A., Obland, M. D., Cook, A. L., Harper, D. B.,
429 Burton, S. P., Shinozuka, Y., McNaughton, C. S., Clarke, A. D., Redemann, J., Russell, P. B., Livingston,
430 J. M. and Kleinman, L. I.: NASA LaRC airborne high spectral resolution lidar aerosol measurements
431 during MILAGRO: observations and validation, *Atmos. Chem. Phys.*, 9(14), 4811–4826, 2009.
- 432 Schwarz, K., Cermak, J., Fuchs, J. and Andersen, H.: Mapping the Twilight Zone—What We Are
433 Missing between Clouds and Aerosols, *Remote Sensing*, 9(6), 577, 2017.
- 434 Shinozuka, Y. and Redemann, J.: Horizontal variability of aerosol optical depth observed during the
435 ARCTAS airborne experiment, *Atmos. Chem. Phys.*, 11(16), 8489–8495, 2011.
- 436 Shinozuka, Y., Johnson, R. R., Flynn, C. J., Russell, P. B., Schmid, B., Redemann, J., Dunagan, S. E.,
437 Kluzek, C. D., Hubbe, J. M., Segal-Rosenheimer, M., Livingston, J. M., Eck, T. F., Wagener, R.,
438 Gregory, L., Chand, D., Berg, L. K., Rogers, R. R., Ferrare, R. A., Hair, J. W., Hostetler, C. A. and
439 Burton, S. P.: Hyperspectral aerosol optical depths from TCAP flights, *J. Geophys. Res. D: Atmos.*,
440 2013JD020596, 2013.
- 441 Shinozuka, Y., Saide, P. E., Ferrada, G. A., Burton, S. P., Ferrare, R., Doherty, S. J., Gordon, H., Longo,
442 K., Mallet, M., Feng, Y., Wang, Q., Cheng, Y., Dobracki, A., Freitag, S., Howell, S. G., LeBlanc, S.,
443 Flynn, C., Segal-Rosenhaimer, M., Pistone, K., Podolske, J. R., Stith, E. J., Bennett, J. R., Carmichael, G.
444 R., da Silva, A., Govindaraju, R., Leung, R., Zhang, Y., Pfister, L., Ryoo, J.-M., Redemann, J., Wood, R.
445 and Zuidema, P.: Modeling the smoky troposphere of the southeast Atlantic: a comparison to ORACLES
446 airborne observations from September of 2016, *Aerosols/Field Measurements/Troposphere/Chemistry*
447 (chemical composition and reactions), doi:10.5194/acp-2019-678, 2019.
- 448 Shipley, S. T., Tracy, D. H., Eloranta, E. W., Trauger, J. T., Sroga, J. T., Roesler, F. L. and Weinman, J.
449 A.: High spectral resolution lidar to measure optical scattering properties of atmospheric aerosols. 1:
450 Theory and instrumentation, *Appl. Opt.*, 22(23), 3716–3724, 1983.
- 451 Stier, P., Schutgens, N. A. J., Bellouin, N., Bian, H., Boucher, O., Chin, M., Ghan, S., Huneeus, N.,
452 Kinne, S., Lin, G., Ma, X., Myhre, G., Penner, J. E., Randles, C. A., Samset, B., Schulz, M., Takemura,
453 T., Yu, F., Yu, H. and Zhou, C.: Host model uncertainties in aerosol radiative forcing estimates: results
454 from the AeroCom Prescribed intercomparison study, *Atmos. Chem. Phys.*, 13(6), 3245–3270, 2013.
- 455 Várnai, T. and Marshak, A.: Satellite Observations of Cloud-Related Variations in Aerosol Properties,
456 *Atmosphere*, 9(11), 430, doi:10.3390/atmos9110430, 2018.
- 457 Virkkula, A.: Correction of the Calibration of the 3-wavelength Particle Soot Absorption Photometer (3λ
458 PSAP), *Aerosol Sci. Technol.*, 44(8), 706–712, 2010.
- 459 Waquet, F., Peers, F., Ducos, F., Goloub, P., Platnick, S., Riedi, J., Tanré, D. and Thieuleux, F.: Global
460 analysis of aerosol properties above clouds, *Geophys. Res. Lett.*, 40(21), 5809–5814, 2013.
- 461 Wilcox, E. M.: Stratocumulus cloud thickening beneath layers of absorbing smoke aerosol, *Atmos. Chem.*



- 462 Phys., 10(23), 11769–11777, 2010.
- 463 Winker, D. M., Vaughan, M. A., Omar, A., Hu, Y., Powell, K. A., Liu, Z., Hunt, W. H. and Young, S. A.:
464 Overview of the CALIPSO Mission and CALIOP Data Processing Algorithms, J. Atmos. Ocean.
465 Technol., 26(11), 2310–2323, 2009.
- 466 Zuidema, P., Redemann, J., Haywood, J., Wood, R., Piketh, S., Hipondoka, M. and Formenti, P.: Smoke
467 and clouds above the southeast Atlantic: Upcoming field campaigns probe absorbing aerosol's impact on
468 climate, Bull. Am. Meteorol. Soc., 97(7), 1131–1135, 2016.
- 469



470

Table 1. Properties and instruments used in this study and the altitudes they refer to.

Property	September 2016 on the ER2 aircraft		August 2017 and October 2018* on the P3 aircraft	
	Instrument	Altitude	Instrument	Altitude
cloud top height (CTH)	HSRL-2	limited to ≤ 3241 m in this study	HSRL-2	no higher than 500 m below the P3 and ≤ 3241 m
aerosol optical depth above cloud top height (AOD _{ct})	HSRL-2	from ~50 m above the CTH to 14 km	4STAR HSRL-2 and 4STAR	from the P3 to top of atmosphere (TOA), when the P3 is 500-1500 m above CTH from ~50 m above the CTH to TOA, except 0-1500 m below the P3, when the P3 is >1500 m above CTH
extinction coefficient, single scattering albedo, submicron non-refractory organic mass, number concentration	-	-	nephelometer, PSAP, HR-ToF AMS and condensation particle counter	at the P3 when the P3 is 500-1500 m above CTH

471

* One day in September 2017 and two days in September 2018 are also included.

472

- Not presented in this study. Observations were made from the P3, away from the ER2 for most

473

cases.

474

475

476



477

Table 2. Statistics on the cloudy-clear differences

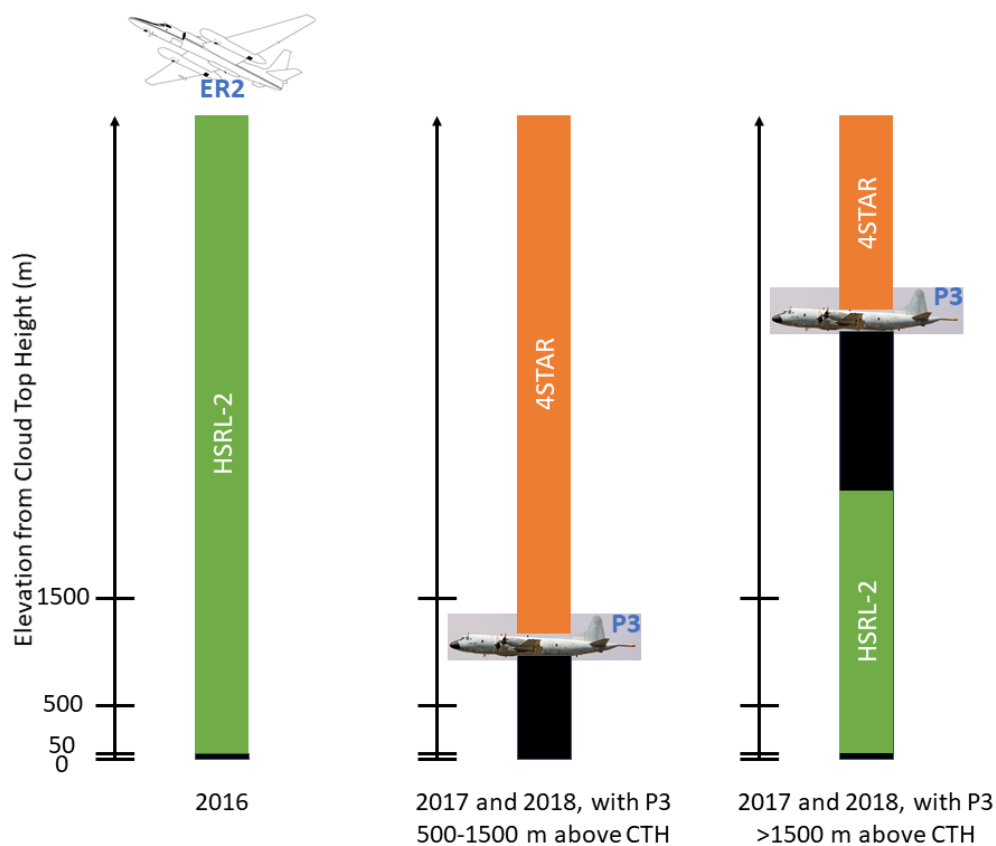
Sampling*	Mean Difference	RMSD	p	Number of Pairs
532 nm AOD _{ct}				
2-6 km	-0.00	0.01	0.08	66
4-12 km	-0.01	0.02	0.23	18
box means	+0.02	0.12	0.23	54
log ₁₀ 532 nm AOD _{ct}				
2-6 km	-0.00	0.01	0.15	66
4-12 km	-0.00	0.02	0.27	18
box means	+0.05	0.19	0.07	54
Angstrom Exponent of AOD _{ct}				
2-6 km	-0.04	0.11	0.00	53
4-12 km	-0.02	0.05	0.08	16
box means	-0.02	0.10	0.14	54
In Situ 550 nm Extinction Coefficient (Mm ⁻¹)				
2-6 km	-0.2	3.0	0.87	7
4-12 km	-3.6	5.1	0.31	3
box means	+19.0	67.9	0.18	24
In Situ 550 nm Single Scattering Albedo				
2-6 km	-0.00	0.01	0.14	7
4-12 km	-0.01	0.01	0.35	3
box means	-0.00	0.05	0.99	24
Submicron Non-refractory Aerosol Organic Mass (µgm ⁻³)				



2-6 km	+0.1	0.5	0.75	9
4-12 km	-0.4	0.6	0.38	3
box means	+1.2	4.4	0.14	28
Number Concentration of Particles >10 nm (cm ⁻³)				
2-6 km	5	59	0.82	10
4-12 km	-110	121	0.09	3
box means	614	1411	0.01	31

478 * Either the temporal separation from cloud edges or box means.

479



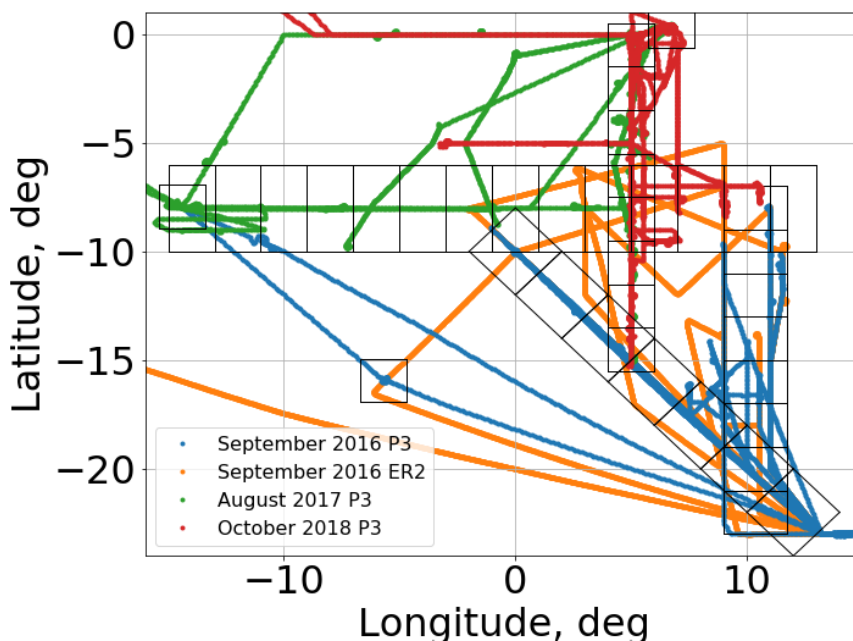
480

481

Figure 1. AOD above cloud top height (AOD_{ct}). See text and Table 1 for details.



482



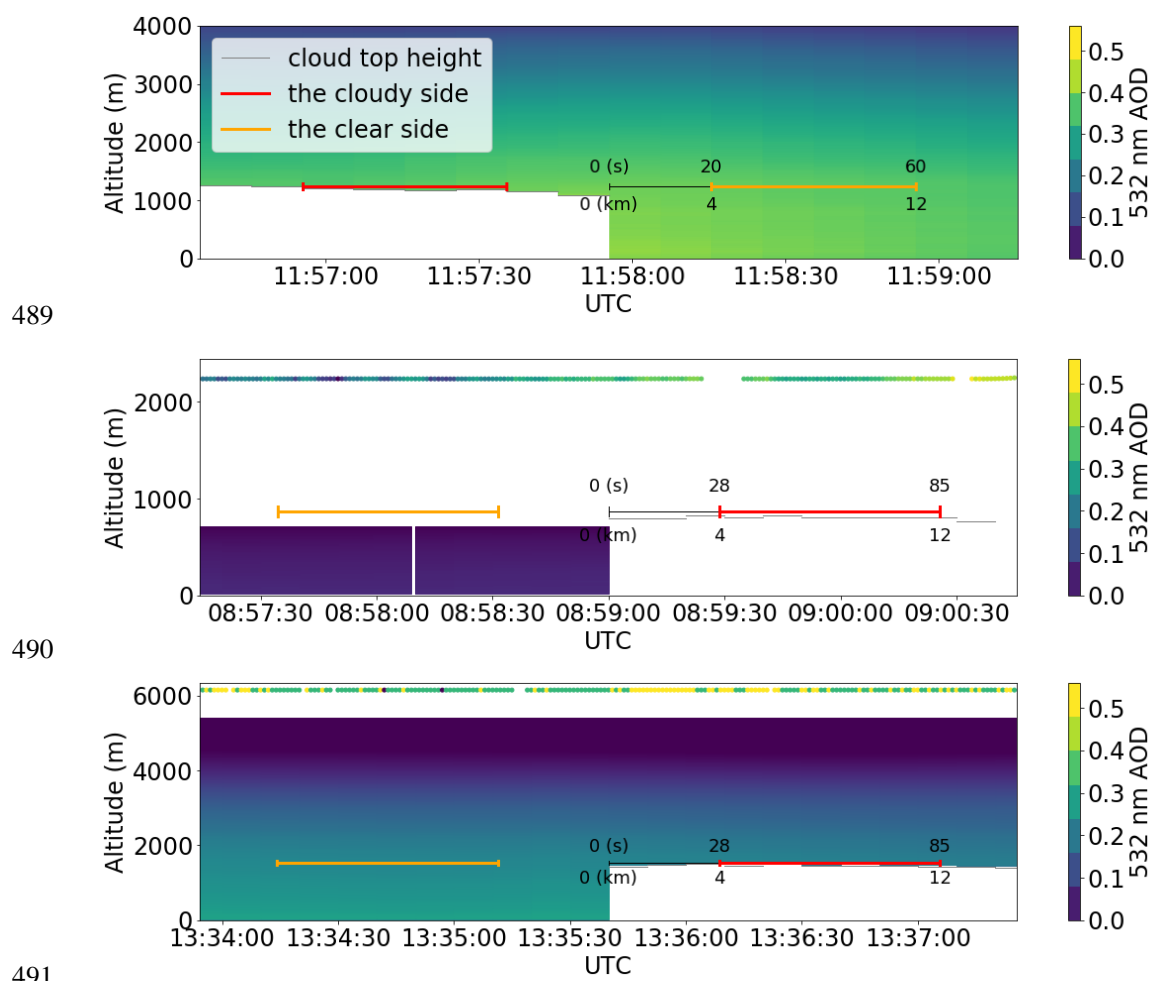
483

484 **Figure 2. The flight paths of ORACLES. The boxes for meso-scale monthly-mean**
485 **sampling are superimposed.**

486

487

488



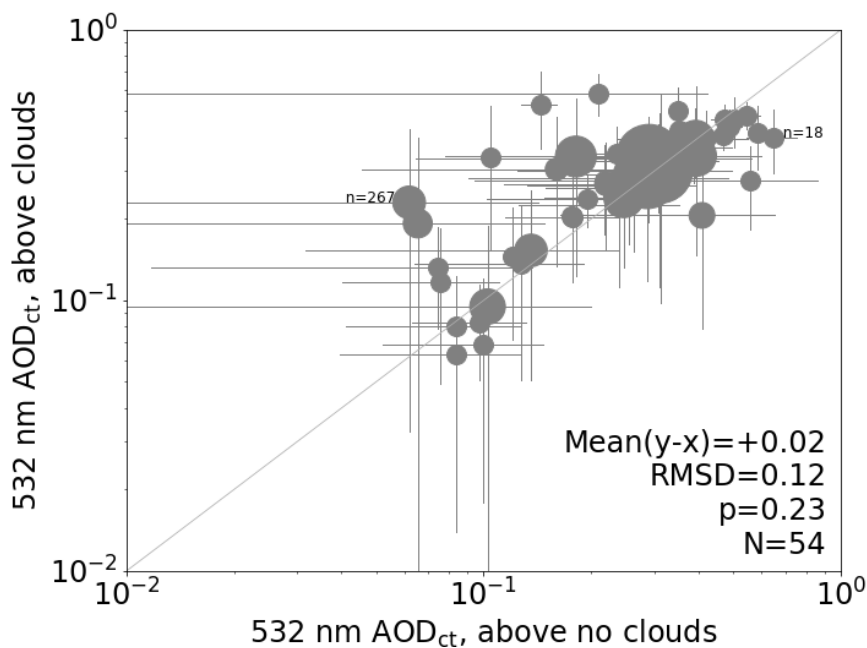
492 **Figure 3. (a) Local-scale near-synchronous sampling based on the HSRL-2 cloud top height**
 493 **(CTH) product. In this subset of the ER2 flight on September 12, 2016, a cloud edge is found**
 494 **at 11:57:56. The cloudy and clear side, each with horizontal separation of 4-12 km measured**
 495 **from cloud edge, are marked by red and orange lines, respectively. The HSRL-2 AOD**
 496 **profiles are given for altitudes from ~50 m above the CTH. (b) An example of local-scale**
 497 **near-synchronous sampling from the P3 aircraft with both HSRL-2 and 4STAR onboard.**
 498 **With the P3 500-1500 m above the CTH, as is the case with this example from October 5,**
 499 **2018, we use 4STAR AOD only. The 4STAR AOD is indicated at the P3 altitudes just above**
 500 **2000 m but refers to all altitudes above them. (c) Another example of local-scale near-**
 501 **synchronous sampling from the P3 aircraft with both HSRL-2 and 4STAR onboard. For the**
 502 **time periods when it flew >1500 m above the CTH, as is the case for this example from**



503 **October 15, 2018, the 4STAR AOD, indicated at the P3 altitudes just above 6000 m, is added**
504 **to the HSRL-2 AOD at ~50 m above the CTH.**

505

506



507

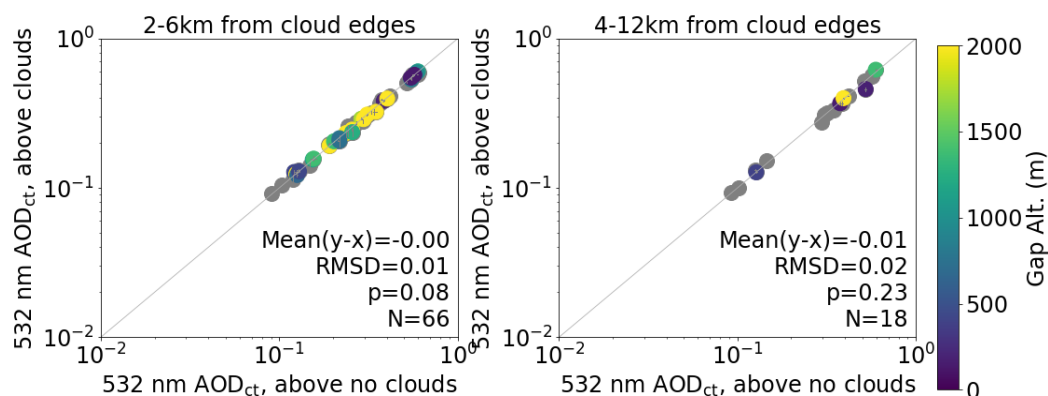
508 **Figure 4. The meso-scale monthly-mean samples of the AOD above cloud top height.**
509 **Each marker represents the mean over a box shown in Fig. 2. The bar represents the**
510 **±1 standard deviation range. The marker size is proportional to the number (n) of 10**
511 **s measurements, the fewer of the cloudy and clear groups.**

512

513

514

515

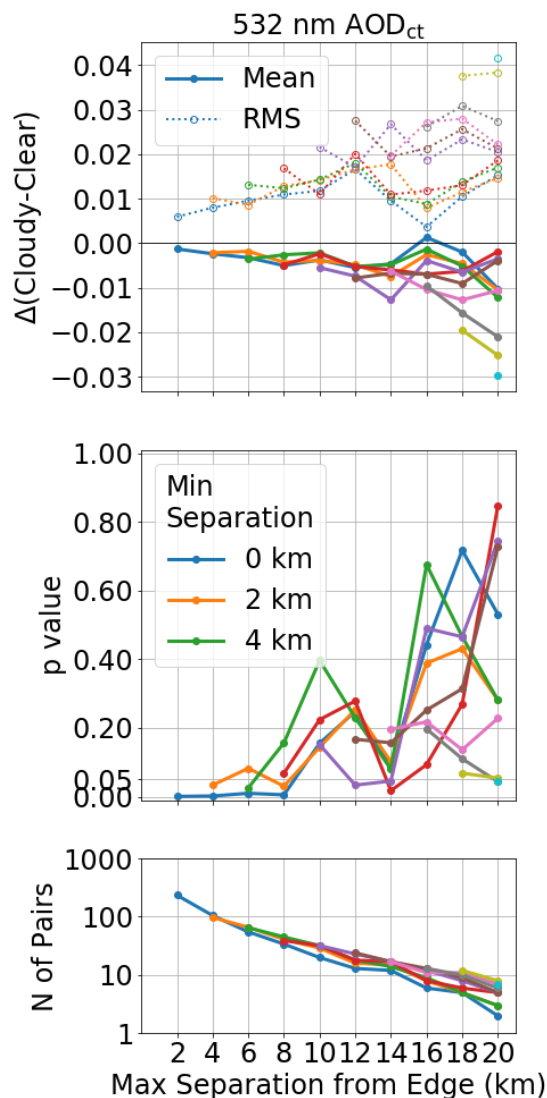


516
517 **Figure 5. (a) The local-scale near-synchronous samples of the AOD above cloud top height.**
518 **Each marker represents the mean over the cloudy and clear sides of a cloud edge, each 2-6**
519 **km from the edge. The bars indicate the standard deviation of the measurements in each**
520 **side, almost all of them too short to be discernible. (b) Same as (a) except for the horizontal**
521 **separation of 4-12 km.**

522

523

524



525

526 **Figure 6. (a) The mean and root-mean-square deviations of the AOD above cloud top**
527 **between the cloudy and clear sides of cloud edges. Each side is defined by the horizontal**
528 **separation from cloud edge. The maximum separation (e.g., 12 km in Fig. 3) is indicated on**
529 **the x axis. Each line represents the minimum temporal separation (e.g., 4 km in Fig. 3) of 0,**
530 **2, 4, ..., 18 km in descending order of line length. (b) The p values determined through the**
531 **paired t-test. (c) the number of cloudy/clear pairs.**